Molecular BioSystems

Accepted Manuscript

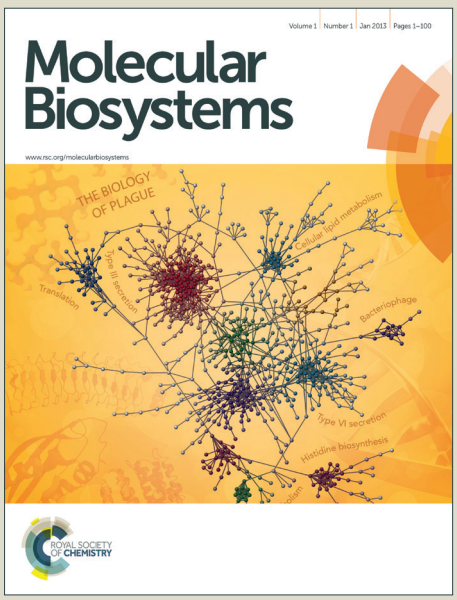

ROYAL SOCIETY OF CHEMISTRY

www.rsc.org/molecularbiosystems

Plasma metabolic profiling after cortical spreading depression in a transgenic mouse model of hemiplegic migraine by capillary electrophoresis - mass spectrometry

Reinald Shyti [a,Δ], Isabelle Kohler [b, Δ], Bart Schoenmaker [b], Rico J. E. Derks [b], Michel D. Ferrari [c], Else A. Tolner [c], Oleg A. Mayboroda [b, #,*], Arn M.J.M. van den Maagdenberg [a,c, #]

[a]: Department of Human Genetics, Leiden University Medical Center, Leiden, The Netherlands

[b]: Center for Proteomics and Metabolomics, Leiden University Medical Center, Leiden, The Netherlands

[c]: Department of Neurology, Leiden University Medical Center, Leiden, The Netherlands

[Δ, #]: equal contribution

***Address of correspondence**

Oleg A. Mayboroda, Center for Proteomics and Metabolomics, Leiden University Medical Center, PO Box 9600, 2300 RC Leiden, The Netherlands

Tel: +31-71-526-63-95

Fax: +31-71-526-69-07

E-mail: o.a.mayboroda@lumc.nl

Table of contents

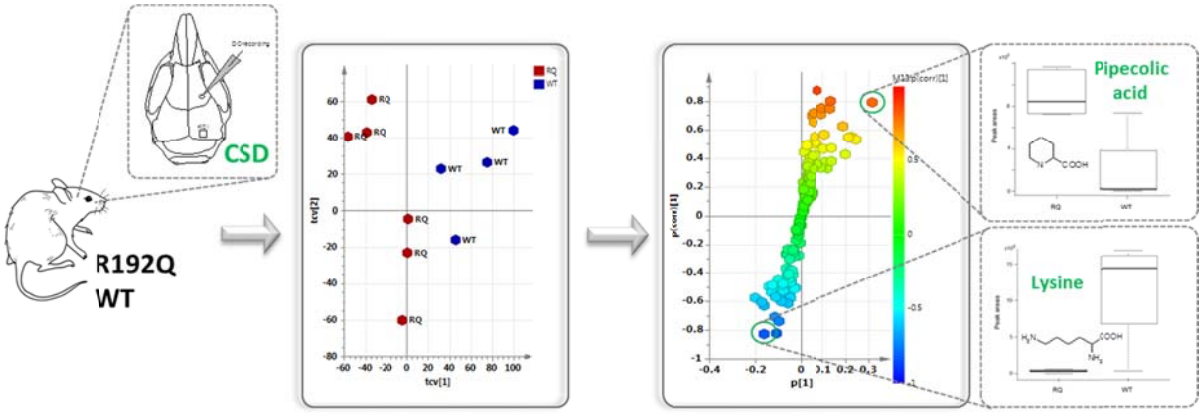

Cortical spreading depression-induced brain metabolic changes have been captured in plasma of a transgenic migraine mouse model of familial hemiplegic migraine using CE-MS and multivariate data analysis.

Abstract

Migraine is a common brain disorder characterized by recurrent attacks of severe headaches and other neurological symptoms. In one-third of patients headaches are accompanied by auras, which consist of transient visual and sensory disturbances, believed to be caused by cortical spreading depression (CSD). CSD is characterized by a wave of neuronal and glial depolarization with concomitant changes in metabolite concentrations in brain and cerebrospinal fluid. It remains unknown whether CSD-induced brain metabolic changes can be captured outside the central nervous system, *i.e.*, in peripheral fluids. This study investigated plasma metabolic changes in transgenic mice that harbor a gene mutation in voltage-gated $Ca_V2.1$ Ca^{2+} channels previously identified in patients with familial hemiplegic migraine, a subtype of migraine with aura. The use of a mouse model allows investigation of molecular changes occurring shortly after CSD, which is notoriously difficult in patients. Capillary electrophoresis - mass spectrometry was used for the analysis of plasma samples to obtain, for the first time, a comprehensive view of molecular changes immediately after experimentally induced CSD. Multivariate data analysis showed a clear distinction between profiles of transgenic and wild-type animals after CSD. Two metabolites considered important for this discrimination were tentatively identified as being lysine and its by-product pipecolic acid with an additional confidence brought by hydrophilic interaction chromatography combined with tandem mass spectrometry. The changed metabolites suggest a compensatory increase in GABAergic neurotransmission upon enhanced excitatory neurotransmission. These results show that CSD induces metabolic remodeling in transgenic migraine mice that can be captured and measured in plasma.

Keywords

Cortical spreading depression; capillary electrophoresis; familial hemiplegic migraine; mass spectrometry; lysine; pipecolic acid.

Abbreviations

α-ASAA, α-aminoadipic semialdehyde; **BGE**, background electrolyte; **CE**, capillary electrophoresis; **CNS**, central nervous system; **CSF**, cerebrospinal fluid; **CSD**, cortical spreading depression; **DA**, discriminant analysis; **EIC**, extracted ion chromatogram; **ESI**, electrospray ionization; **EOF**, electro-osmotic flow; **EtOH**, ethanol; **FHM**, familial hemiplegic migraine; **GABA**, γ-hydroxybutyric acid; **HILIC**, hydrophilic interaction chromatography; **HMDB**; Human Metabolome Database; ***i*-PrOH**, isopropanol; **MeCN**, acetonitrile; **MeOH**, methanol; **MS**, mass spectrometry; **MS/MS**, tandem mass spectrometry; **OPLS**; orthogonal partial least square; **PA,** pipecolic acid; **PCA**, principal component analysis; **PDE**, pyridoxine-deficient epilepsy; **PLS**, partial least square; **PP**, protein precipitation; **PR**, product ion; **QC**, quality control; **QqQ**, triple quadrupole; **SPE**, solid-phase extraction; **TOF**, time-of-flight; **t-ITP**, transient isotachophoresis; **VIP**, Variable Influence on Projection; **WT**, wild-type.

1. Introduction

Migraine is a common debilitating brain disorder characterized by episodic recurrent attacks of severe headaches often accompanied by nausea, vomiting, photophobia, and phonophobia[1, 2]. In one-third of patients attacks are accompanied by transient neurological dysfunction called aura that consists of visual, sensory or aphasic symptoms. Familial hemiplegic migraine (FHM), a monogenic subtype of migraine with aura with reversible pronounced motor weakness during the aura, is considered a valid model for common forms of migraine[3]. FHM type 1 is caused by mutations in the *CACNA1A* gene that encodes the pore-forming α_1 subunit of neuronal $Ca_V2.1$ (P/Q-type) voltage-gated calcium channels[4-7]. The underlying cause of the aura is cortical spreading depression (CSD), which consists of a wave of glial and neuronal depolarization that slowly propagates through the cortex and is followed by a long-lasting (*ca.* 1 hour) neuronal silencing. Experiments in animals have shown that CSD can activate trigeminovascular pathways in the brainstem involved in headache generation[8, 9], but such evidence is lacking in humans. CSD leads to a disruption of cellular ionic balance and is associated with changes in extracellular levels of ions, neurotransmitters, and metabolites[10, 11]. Furthermore, it has been shown that a CSD event can change blood-brain barrier permeability[12], which may indicate that CSD events and their consequences may be traced beyond the central nervous system (CNS), *e.g.*, in peripheral fluids such as blood or urine. Metabolomics appears a logical approach for testing this assumption; indeed, the response of an organism to any biological effect is ultimately reflected in alterations of metabolic composition of body fluids. Profiling of CSD-induced molecular changes may give relevant molecular insight into the pathophysiological mechanisms of migraine and lead to relevant (putative) biomarkers for diagnosis, monitoring, or prognosis of migraine events in patients. Surprisingly, even though the clinical importance of metabolomics-based studies has been widely demonstrated for various neurological disorders, migraine remains a largely unexplored area[13].

Performing metabolomics studies in mice poses technical challenges that need to be addressed. For instance, non-terminal blood collection provides only minute amounts (*i.e.*, few µL) of plasma, a miniaturized analytical workflow is thus mandatory. Capillary electrophoresis hyphenated to mass spectrometry (CE-MS) presents numerous advantages, including high-separation efficiency and selectivity, as well as low sample and solvent consumption. The feasibility of CE-MS as an analytical method for metabolic profiling of the volume-restricted samples has been shown multiple times; it is particularly well-suited for the analysis of polar and ionizable compounds, such as amino acids, phosphorylated compounds, tricarboxylic acid cycle intermediates, as well as nucleosides and nucleotides in biosamples[14-17]. The high sensitivity and resolution required for such

bioanalytical applications can be reached by using online sample preconcentration techniques and a sheathless nanospray ionization interface. A prototype based on a porous sheathless interface, first proposed by Moini[18], has been successfully used for metabolomics applications[19-21]. This sheathless interface has shown to display a mass-flux sensitive response at flow rates lower than 25 nL/min, suggesting a maximum sensitivity and reduced ion suppression at the very low flow rates usually observed with CE[22].

In this study, CE-MS was used for metabolic profiling of plasma from a FHM1 transgenic mouse model carrying a R192Q missense mutation that was introduced in the *CACNA1A* gene[23]. The mutant mice exhibit migraine-relevant features including an increased susceptibility to CSD that is the consequence of enhanced excitatory neurotransmission due to hyperactive $Ca_V2.1$ channels[23-25]. CSD-induced metabolite changes significantly differed between mutants and wild-type (WT) control animals. Hydrophilic interaction chromatography (HILIC) combined with tandem mass spectrometry (MS/MS) was used for platform-independent and orthogonal confirmation of the identity of lysine and pipecolic acid (PA), the two metabolites that were considered important for the discrimination of mutant and wild-type metabolite profiles. Changed levels of lysine and PA may reflect a compensatory increase in GABAergic neurotransmission as a consequence of enhanced excitatory neurotransmission that is particularly prominent in mutant mice upon CSD.

2. Materials and Methods

2.1. Chemicals

Potassium chloride, sodium chloride, sodium hydroxide, methanol (MeOH), ethanol (EtOH), isopropanol (*i*-PrOH), 28% ammonium hydroxide (*m/v*), L-lysine monohydrochloride, and L-PA were of analytical grade and purchased from Sigma-Aldrich (Schnelldorf, Germany). Water and acetonitrile (MeCN) were of LC-MS grade and were obtained from Sigma-Aldrich. Formic and acetic acid were of ULC-MS grade and were purchased from Biosolve (Valkenswaard, The Netherlands).

2.2. Animals

Male 2- to 4-month-old FHM1 R192Q and wild-type (WT) control mice were used and genotyped as previously described[23]. Mice were kept in a standard 12:12 light dark cycle; water and food were available *ad libitum*. All the animal experiments were approved by the Animal Experiment Ethics Committee of Leiden University Medical Centre.

2.3. Induction and recording of cortical spreading depression

Mice were anesthetized using 4% isoflurane in pressurized air (20% O_2 and 80% N_2) for induction and 1.5% for maintenance. Mice were placed in a stereotactic frame (David Kopf, Tujunga, CA, USA) and a midline incision was made to expose the skull. Two burr holes were drilled with a microdriller at the following coordinates from bregma: 3.5 mm posterior and 2 mm lateral for CSD induction in the occipital cortex and 0.5 mm anterior and 2 mm lateral for CSD recording in the frontal cortex. CSD events were induced by application of a cotton ball soaked in 1M KCl over the dura for 30 s, immediately removed prior to thorough washing with saline solution. In sham-operated mice, a cotton ball soaked in 1M NaCl was applied for 30 s, immediately removed prior to thorough washing with saline solution. This procedure was repeated 7 times each with a 5-min interval for both CSD- and sham-operated mice. The experimental design, illustrated in Supplementary Figure 1, included 24 mice, *i.e.*, two groups consisting of 12 sham- and 12 CSD-operated mice, each group containing 6 WT and 6 R192Q animals. CSD events were measured as DC-potential changes that were recorded at 300-µm depth using a glass electrode filled with 150 mM NaCl in the frontal cortex. Data were sampled at 200 Hz, amplified (10X) and low-pass-filtered (100 Hz) using Powerlab (AD Instruments Inc, Colorado Springs, CO, USA).

2.4. Sample collection and preparation

Five minutes after the 7th CSD (in case of KCl application) or 7th sham (in case of NaCl application), mice were decapitated and a minimum of 40 µL of blood was collected from the trunk in heparinized blood collection capillaries (Sarstedt Microvette CB 300, Nümbrecht, Germany). Plasma samples were obtained after centrifugation of blood for 10 min with 4000 rpm at 4^{o}C and then snap-frozen in liquid N_2 and stored at -80^{o}C. Prior to CE-MS analysis, plasma samples were thawed at room temperature. Protein precipitation (PP) was carried out with addition of cold EtOH to the plasma (3:1, *v/v*) followed by vortex agitation. After 20 min, samples were centrifuged for 10 min at 4000 rpm prior to the collection of supernatant and its evaporation to dryness. The obtained dried extracts were dissolved by addition of 100 mM ammonium acetate at pH 4.0 to a volume corresponding to the original one. The prepared samples were randomized prior to CE-MS analysis, which also included quality control (QC) samples consisting of a pool of all plasma samples prepared in the same way to evaluate the analytical variability of the CE-MS experimental set-up.

2.5. Capillary electrophoresis – mass spectrometry

2.5.1. CE-MS experiments

CE experiments were performed using a PA800 Plus instrument (Beckman Coulter, Brea, CA, USA) equipped with a temperature-controlled sample tray, capillary cooling liquid, and a power supply able to deliver up to 30 kV. CE separations were carried out with neutrally-coated capillaries (30 µm i.d. × 150 µm o.d. × 100 cm) consisting of a bilayer with polyacrylamide as the outer layer and the end proximal to the mass analyzer made porous to ion flow, in development and supplied by Beckman Coulter at the time of this study. CE was hyphenated to a MaXis 4G UHR-TOF mass analyzer (Bruker Daltonics, Bremen, Germany) *via* a porous CE-electrospray (ESI)-MS sheathless interface. The prototype interface set up as well as daily system suitability tests are described in details elsewhere[22, 26]. The background electrolyte (BGE) was composed of 10% acetic acid (*v/v*). Samples were hydrodynamically introduced at 2.5 psi for 65 s (corresponding to 3% of the capillary volume, 25 nL) using a transient isotachophoresis (t-ITP) online pre-concentration previously described[26]. Separation was carried out in 65 min with an applied voltage of 25 kV and a pressure of 2 psi to ensure the ESI spray stability. MS acquisition was performed in ESI positive mode over the range 50 to 1500 *m/z* with an acquisition rate of 1 Hz. ESI capillary voltage was set at -1200 V and drying flow rate and temperature at 2

L/min and 180°C, respectively. A hydro-organic solution of H_2O/*i*-PrOH 50:50 (*v/v*) containing sodium formate clusters was infused at the beginning of each analysis to allow for mass recalibration.

2.5.2. Data analysis

All MS data files were recalibrated based on sodium formate *m/z* clusters. The CE-MS data files were exported in *mzxml* format and aligned with the in-house developed alignment algorithm msAlign2 available on www.ms-utils.org/msalign2 [27]. Peak picking was performed with XCMS package (The Scripp Research Institute, La Jolla, CA, USA) based on the *centWave* algorithm using the following settings: maximal tolerated *m/z* deviation in consecutive scans, 5 ppm; electrophoretic peak width, 5-15 s; scan range to process, 70-1500 *m/z*; noise, 15,000; prefilter step, at least 3 peaks with intensity >20,000; *m/z* center of the feature, *wMean* (intensity weighted mean of the feature *m/z* values); signal-to-noise ratio threshold, 50; minimum difference in *m/z* for peaks with overlapping migration time, 0.05 min; integration method, peak limits found through descent on the Mexican hat filtered data; no Gaussian fitted to each peak[28, 29]. Probabilistic Quotient Normalization method was used to account for the dilution of the samples[30]. Data were mean centered and a square root transformation was used to correct for the heteroscedasticity.

Principal component analysis (PCA), partial least squares discriminant analysis (PLS-DA), and orthogonal partial least squares discriminant analysis (OPLS-DA) were computed using SIMCA-P+ software version 12.0 (Umetrics, Umeå, Sweden). The validity of the PLS-DA model was checked using a permutation test containing 200 iterations. Features responsible for the separation between classes in OPLS-DA were determined based on the S-plot visualization method and the Variable Influence on Projection (VIP) values, which both highlight the importance of the variables for the classification. In order to identify the classifiers of interest, rational chemical formulas were generated based on the internally calibrated monoisotopic mass within 5 ppm mass error and submitted to METLIN Metabolite Search (http://metlin.scripps.edu)[31] and Human Metabolome Database (HMDB, http://www.hmdb.ca)[32]. The confirmation of the identity of metabolites of interest was carried out by HILIC-MS/MS.

2.6. Hydrophilic interaction chromatography-tandem mass spectrometry

HILIC-MS/MS experiments were performed with a LC-MS Advance™ UHPLC hyphenated to an EVOQ Elite™ Triple Quadrupole (QqQ), both from Bruker Daltonics. Confirmatory analyses were carried out with a Luna NH_2 column (Phenomenex, Utrecht, The Netherlands) of 100 mm × 2.00 mm i.d., 3 µm, and 100 Å. The

mobile phase was composed of a 20 mM ammonium acetate buffer at pH 9.0 (A) and MeCN (B). The flow rate was set to 600 µL/min with the following gradient profile: 95% B for 1 min, 95-5% B in 5 min, and 5% B for 1 min. Equilibration of the column was performed with 95% B for 5 min. Analyses were carried out at 40°C. MS/MS experiments were performed in positive ESI mode with a collision energy of 10 eV and a dwell time of 200 ms. ESI source parameters were 4500 V for the ESI capillary voltage, 20 V and 250°C for the cone gas voltage and temperature, respectively, 20 V and 300°C for the probe gas voltage and temperature, respectively, and 20 psi for the nebulizer gas. N_2 was used for collision-induced dissociation at a pressure of 1.5 mTorr. Sample preparation included plasma PP prior to solid-phase extraction (SPE). PP was carried out by adding 1.5 mL of MeOH to 500 µL of pooled plasma collected from naïve WT control mice and centrifuged at 13,000 rpm for 10 min. The supernatant was collected and basified (*ca.* pH 12) by adding 2 mL of a mixture of NH_4OH/H_20 5:95 (*v/v*). SPE was performed on precipitated sample with Strata Strong Anion Mixed Mode (Strata-X-A, Phenomenex) cartridges containing 100 mg sorbent mass. SPE cartridges were first conditioned with 1 mL MeOH and equilibrated with 1 mL of NH_4OH/H_20 5:95 (*v/v*) prior to the loading of basified sample. The first and second washing step were performed with 1 mL of NH_4OH/H_20 5:95 (*v/v*) and 1 mL of MeOH, respectively. Compounds of interest were then eluted with 1 mL of a mixture of HCOOH/MeOH 2:98 (*v/v*). The organic eluate was evaporated to dryness and reconstituted in 25 µL of a solution of MeCN/0.1 M HCl 9:1 (*v/v*). Two µL of this solution were eventually injected for subsequent HILIC-MS/MS experiments.

3. Results and Discussion

3.1. Plasma metabolic profiling by CE-MS

In order to reach the highest sensitivity and separation efficiency, leading to an enhanced plasma metabolic coverage, an integrated CE nanospray MS approach was used in combination with transient t-ITP online pre-concentration[26]. The use of neutrally-coated capillaries, which almost entirely suppress the electro-osmotic flow (EOF), also allowed for the highest separation efficiencies while keeping the CE effluent to very low flow rates (<25 nL/min) which are necessary to observe a mass-flux sensitive detector response[22]. A typical base peak electropherogram obtained with the analysis of precipitated mouse plasma is shown in Fig. 1.

Compared to widely-used chromatographic techniques, CE-MS, especially at very low EOF, suffers from a poorer migration time repeatability which can affect the statistical data analysis and, eventually, the identification of putative compounds of interest. Therefore, most of the available algorithms and software packages previously developed for LC-MS and routinely used for non-linear correction of retention times are usually not fully adapted to CE-MS data. Prior to subsequent data pre-processing and analysis, CE-MS data were thus aligned using a dedicated, in-house, and open source alignment tool, msalign2[27].

The analytical consistency of the CE-MS workflow was evaluated *via* analysis of QCs composed of a pool of all samples repeatedly analyzed at regular intervals throughout the sequence runs[33, 34]. To this end, a PCA model was built on the whole data set, *i.e.*, 20 samples and all QCs. Four samples, *i.e.*, two from the CSD and two from the sham group, were discarded prior to the data analysis as no satisfactory data were acquired due to instrumental issues. As shown by the score plot obtained for the first two principal components (covering 50% of the total variation) presented in Supplementary Figure 2, the variation present in the group of mouse samples was much larger than the variation between QCs. The analytical variability was thus considered having a negligible influence on the data matrix. QCs were then removed from the data set for subsequent data analysis.

The initial PCA analysis of the entire data set did not show any trend or tendency relevant to the experimental design (data not shown). Thus, in order to dissect CSD-triggered differences in the metabolic composition of plasma samples of FHM1 R192Q mice in comparison to WT mice, the PCA models were built for sham and CSD mice separately (Fig. 2). Visual inspection of the PCA plots revealed important differences between the models. Fig. 2.A presents the score-plot of the first two principal components for PCA obtained for the combined FHM1 R192Q and WT sham group where the samples were randomly distributed. This result was

anticipated as no CSD event was induced in this group of mice. However, the PCA score plot obtained for the combined FHM1 R192Q and WT CSD group (Fig. 2.B) showed a clear trend in sample clustering. Two PLS-DA models (*i.e.*, for sham and CSD groups) with WT and FHM1 R192Q mice as class identifiers were built to confirm these observations. As expected, the PLS-DA model built on sham samples proved to be statistically poor, while the statistical descriptors of the CSD data indicated a solid model (R^2X cum = 0.417, R^2Y cum = 0.996, Q^2 = 0.712). Fig. 3.A presents the cross-validated score-plot PLS-DA model built on CSD data. The metabolites responsible for this classification were highlighted by OPLS-DA regression and the derived S-plot (Fig. 3.B). The S-plot is a visualization method that combines the modelled covariance (X-axis) and modelled correlation (Y-axis) from the OPLS-DA on a scatter plot, allowing for pinpointing of interesting variables. The variables showing the highest p and $p(corr)$ values are considered the most relevant metabolites for the classification between samples. According to the S-plot and Variable Importance on Projection (VIP) values, two metabolites were ranked as the most important variables responsible for the separation between FHM1 R192Q and WT groups after CSD. The first metabolite (VIP value = 4.1), measured at *m/z* 130.0860 with a migration time of 14.5 min, showed a higher peak area in FHM1 R192Q group relative to WT controls, after CSD. Based on the monoisotopic mass, the isotope distribution, the nitrogen rule, the hydrogen/carbo ratio rule[35], as well as research in METLIN Metabolite Search and HMDB public databases, this metabolite was tentatively identified as pipecolic acid ($C_6H_{11}NO_2$, exact *m/z* 130.0863, Δ = 2 ppm), a non-protein imino acid. Another important metabolite responsible for the samples classification (VIP values = 1.1 and 2.1 for most abundant and second most abundant isotope, respectively), biochemically correlated to PA and detected at *m/z* 147.1128 with a migration time of 14.2 min was determined as being lysine ($C_6H_{14}N_2O_2$, exact *m/z* 147.1128, Δ = 0 ppm), which showed a significantly lower peak area in FHM1 R192Q samples compared to WT after CSD. Fig. 4 shows the box-plots constructed for both metabolites with integrated peak areas, highlighting the significant difference observed between FHM1 R192Q and WT plasma after CSD, with significantly higher peak areas for PA (Fig. 4.A) and lower areas for lysine (Fig. 4.B), respectively, in the FHM1 R192Q group compared to WT control.

3.2. Confirmatory analysis by HILIC-MS/MS

The use of an orthogonal analytical technique such as liquid chromatography, *i.e.*, based on a different mechanism of separation than CE, as well as information on the fragmentation pattern *via* MS/MS experiments provides an additional confidence of the identification of both compounds[36]. Contrary to widely used reversed-

phase liquid chromatography, where a poor retention and selectivity is usually observed for metabolites analysis, the HILIC chromatographic mode is well-suited for the analysis of relatively polar compounds[37-40].

HILIC-MS/MS experiments were carried out on a QqQ mass analyzer with standard solutions of L-PA and L-lysine and naïve WT control mouse plasma. As the basal concentration of PA was observed to be relatively low in plasma of WT mice, a sample preconcentration was necessary to reach the sufficient limit of detection for both compounds. The 20-fold preconcentration obtained with the developed PP-SPE procedure based on anion-exchange mechanism allowed for the detection of both compounds in plasma sample. Product ion scan (PR) mode, *i.e.*, where the first quadrupole of the QqQ selects the parent ion(s) then fragmented in the collision cell prior to the detection of fragments in the third quadrupole operating in the full-scan mode, was used for MS/MS acquisition. Fig. 5 shows the extracted ion chromatograms (EICs) obtained for PA (Fig. 5.A) and lysine (Fig. 5.B) in the plasma sample with their respective MS/MS spectra obtained with a collision of energy of 10 eV. The EICs obtained for *m/z* 130 and *m/z* 147 showed similar retention times for both compounds in plasma samples and standard solutions, *i.e.*, 3.22 min and 3.61 min for PA and lysine, respectively. The identity of the compounds was confirmed by comparing the MS/MS spectra obtained for *m/z* 130 and *m/z* 147 in plasma sample versus standard spectra. The MS/MS spectrum observed for PA in plasma showed the molecular ion at *m/z* 130 as well as a fragment at *m/z* 84, which corresponds to the loss of the carboxyl functional group. The MS/MS spectrum of lysine showed the molecular ion at *m/z* 147 as well as fragments at *m/z* 130 and *m/z* 84. The fragment at *m/z* 130 is obtained with the loss of the secondary amine prior to cyclization of the molecule into PA[41] and, rationally, the subsequent loss of the carboxyl group to obtain the fragment at *m/z* 84. According to the Metabolomics Standards Initiative, a definitive (*i.e.*, level 1) compound identification may be obtained by comparing two or more orthogonal properties (*e.g.*, retention time, *m/z* ratio, fragmentation mass spectrum) of an authentic chemical standard *versus* the metabolite(s) of interest[42, 43]. Due to the restricted sample volume available from mice, the orthogonal confirmatory analysis was performed on a WT material only. Therefore, additional studies may be required to increase the confidence in the identification of PA and lysine, although CE data usually provide a strong context for identification of amino acids, and lysine in particular.

3.3. Lysine and pipecolic metabolism and biological implications

In animals and humans, L-lysine has been shown to be predominantly metabolized to saccharopine (ε-*N*-[glutaryl-2]-L-lysine) in peripheral tissues, including liver and kidney, while the brain appears to mainly metabolize this amino acid to the intermediate of reaction L-PA. Both pathways lead to the formation of α-

aminoadipic semialdehyde (α-ASAA), α-aminoadipic acid, and eventually acetyl-Co-A. The primary metabolic function of PA in human and mammals, however, is unknown. Nevertheless, PA was shown to be associated with several diseases, such as pyridoxine-dependent epilepsy, α-ASAA dehydrogenase deficiency, inherited peroxisomal disorders, and chronic liver dysfunction[44, 45].

Peroxisomal disorders are characterized by a defect in peroxisome formation, leading to a deficiency or little activity of the peroxisomal PA oxidase, the enzyme responsible for oxidation of PA. A significant elevation of L-PA plasma concentration (normal range 0.1-4.0 μmol/L) is observed and used for diagnosis purpose in combination with the determination of plasma very-long-chain fatty acids and plasmalogens[46-48].

Pyridoxine-dependent epilepsy (PDE) is a recessive inherited condition that affects the γ-aminobutyric acid (GABA) pathway and is characterized by epileptic seizures that are not controlled with antiepileptic drugs but stop with administration of pharmacological doses of pyridoxine (vitamin B_6)[48-50]. Due to α-ASAA dehydrogenase deficiency caused by pathogenic mutations in the *ALDH7A1* gene, elevated levels of α-ASAA are observed in plasma, CSF, and urine in patients with PDE. Increased concentrations of L-PA have also been observed in plasma (4.3 - 15.3 fold) and CSF (5.6 – 37.2 fold) of patients with PDE [50, 51]. *In vitro* experiments revealed that L-PA serves as a modulator of GABAergic neurotransmission by stimulating GABA release in the synaptic cleft, decreasing its uptake by the synaptosomes, and/or enhancing $GABA_A$ receptor response likely by binding to another site on $GABA_A$ receptor [52-57]. PDE remains up to now the only paroxysmal episodic disorder for which a correlation between plasma PA concentrations and brain events has been shown.

To the best of our knowledge, this is the first time that the lysine degradation pathway is suggested to be involved in migraine pathophysiology. Any relevance for migraine mainly comes from the observation that changes in plasma levels of lysine and PA were different in FHM1 R192Q mutant versus WT control mice after CSD induction only, and not after sham treatment. The higher level of PA after CSD induction in FHM1 R192Q mutant may hypothetically point towards a compensatory mechanism to counteract the effect of excessive glutamatergic neurotransmission *via* an enhancement of inhibitory GABAergic synaptic transmission; perhaps to restore the imbalance in cortical excitatory-inhibitory transmission that occurs with CSD. In this scenario, increased GABAergic synaptic transmission may be an attempt of the brain to restore homeostasis. Increased GABAergic synaptic transmission may be the mere consequence of the excessive glutamatergic neurotransmission and subsequent activation of GABAergic neurons, without direct changes at the level of GABAergic transmission. Indeed, it has been already shown that the FHM1 R192Q mutation increases excitatory glutamatergic neurotransmission while having no effect on inhibitory GABAergic transmission[25].

Enhanced glutamatergic neurotransmission was shown to underlie the increased susceptibility to CSD in FHM1 R192Q mutant mice[25]. Finally, a proteomic analysis of synaptosomes from cortical neurons of FHM1 R192Q mutant mice showed compensatory up-regulation of glutamate transporters[58]. These features seem to suggest that although GABAergic neurotransmission seems not primarily affected in FHM1 R192Q mice, it may kick in as part of the consequences of the enhanced excitatory transmission and may be involved in compensatory actions attempting to restore brain homeostasis, a hypothesis which would fit the episodic nature of migraine. This study also brings out that the mechanisms underlying CSD events can be captured beyond the CNS, for instance in plasma. It thus suggests that the investigation of metabolic changes in peripheral fluids may provide a useful strategy to monitor pathophysiological effects related to migraine that occur in the brain.

4. Concluding remarks

This study investigated the metabolic profiling in plasma of transgenic migraine mice carrying the FHM1 R192Q mutation and WT controls following induction of multiple CSD events. Plasma samples collected after CSD induction were analyzed by CE-MS and highlighted significant changes in concentration of two metabolites in FHM1 R192Q mutant that were tentatively identified as lysine and PA. The relative changes of PA concentration observed in FHM1 mutatn mice compared to WT are consistent with the previsouly shown correlation between PA and inhibitory GABAergic neurotransmission, which in theory may serve to counteract the neuronal excitability and promote homeostasis recovery upon CSD in FHM1 mutant mice. Notably, CSD events appear to induce a metabolic remodeling in peripheral fluids such as plasma. This opens new perspectives in the discovery of putative biomarkers in easily-accessible body fluids to improve the diagnostics and prognosis in migraine, as well as in proposing novel biomolecular targets for the development of new therapies. Further experiments are required to investigate the longitudinal evolution of the metabolic profile underlying CSD in peripheral fluids.

5. Acknowledgements

This work was financially supported by the Dutch Organization for Scientific Research, EU Marie Curie IAPP Program “BRAINPATH” (nr 612360) (A.M.J.M.v.d.M.), EU “EUROHEADPAIN” grant (nr 602633) (M.D.F., A.M.J.M.v.d.M), an LUMC Fellowship (E.A.T.), Marie Curie Career Integration Grant (nr 294233) (E.A.T.) and the Center of Medical System Biology (CMSB) established by the Netherlands Genomics Initiative (NGI)/NWO (A.M.J.M.v.d.M.). I.K. was a recipient of a fellowship (P2GEP3_155633) supported by the Swiss

National Scientific Foundation. Jeff D. Chapman from Beckman Coulter/AB Sciex is acknowledged for the kind loan of CE-MS sheathless prototype and valuable discussions.

6. References

1. P. J. Goadsby, R. B. Lipton and M. D. Ferrari, *N Engl J Med*, 2002, 346, 257-270.
2. ICHD, *Cephalalgia*, 2004, 24 Suppl 1, 9-160.
3. M. D. Ferrari, R. R. Klever, G. M. Terwindt, C. Ayata and A. M. Van den Maagdenberg, *Lancet Neurol*, 2014, 14, 65-80.
4. R. A. Ophoff, G. M. Terwindt, M. N. Vergouwe, R. van Eijk, P. J. Oefner, S. M. Hoffman, J. E. Lamerdin, H. W. Mohrenweiser, D. E. Bulman, M. Ferrari, J. Haan, D. Lindhout, G. J. van Ommen, M. H. Hofker, M. D. Ferrari and R. R. Frants, *Cell*, 1996, 87, 543-552.
5. A. Ducros, C. Denier, A. Joutel, M. Cecillon, C. Lescoat, K. Vahedi, F. Darcel, E. Vicaut, M. G. Bousser and E. Tournier-Lasserve, *N Engl J Med*, 2001, 345, 17-24.
6. B. de Vries, R. R. Frants, M. D. Ferrari and A. M. van den Maagdenberg, *Hum Genet*, 2009, 126, 115-132.
7. A. M. van den Maagdenberg, J. Haan, G. M. Terwindt and M. D. Ferrari, *Curr Opin Neurol*, 2007, 20, 299-305.
8. X. Zhang, D. Levy, V. Kainz, R. Noseda, M. Jakubowski and R. Burstein, *Ann Neurol*, 2011, 69, 855-865.
9. H. Karatas, S. E. Erdener, Y. Gursoy-Ozdemir, S. Lule, E. Eren-Kocak, Z. D. Sen and T. Dalkara, *Science*, 2013, 339, 1092-1095.
10. G. G. Somjen, *Physiol Rev*, 2001, 81, 1065-1096.
11. J. A. Davies, S. J. Annels, B. G. Dickie, Y. Ellis and N. J. Knott, *J Neurol Sci*, 1995, 131, 8-14.
12. Y. Gursoy-Ozdemir, J. Qiu, N. Matsuoka, H. Bolay, D. Bermpohl, H. Jin, X. Wang, G. A. Rosenberg, E. H. Lo and M. A. Moskowitz, *J Clin Invest*, 2004, 113, 1447-1455.
13. L. Lionetto, G. Gentile, E. Bellei, M. Capi, D. Sabato, F. Marsibilio, M. Simmaco, L. A. Pini and P. Martelletti, *J Headache Pain*, 2013, 14, 55.
14. G. Bonvin, J. Schappler and S. Rudaz, *J Chromatogr A*, 2012, 1267, 17-31.
15. I. Kohler, J. Schappler and S. Rudaz, *Anal Chim Acta*, 2013, 780, 101-109.
16. M. G. M. Kok, G. W. Somsen and G. de Jong, *TrAC*, 2014, 61, 223-235.
17. A. Hirayama, M. Wakayama and T. Soga, *TrAC*, 2014, 61, 215-222.
18. M. Moini, *Anal Chem*, 2007, 79, 4241-4246.
19. A. Hirayama, M. Tomita and T. Soga, *Analyst*, 2012, 137, 5026-5033.
20. R. Ramautar, R. Shyti, B. Schoenmaker, L. de Groote, R. J. Derks, M. D. Ferrari, A. M. van den Maagdenberg, A. M. Deelder and O. A. Mayboroda, *Anal Bioanal Chem*, 2012, DOI: 10.1007/s00216-012-6431-7.
21. E. Nevedomskaya, R. Ramautar, R. Derks, I. Westbroek, G. Zondag, I. van der Pluijm, A. M. Deelder and O. A. Mayboroda, *J Proteome Res*, 2010, 9, 4869-4874.
22. J. M. Busnel, B. Schoenmaker, R. Ramautar, A. Carrasco-Pancorbo, C. Ratnayake, J. S. Feitelson, J. D. Chapman, A. M. Deelder and O. A. Mayboroda, *Anal Chem*, 2010, 82, 9476-9483.
23. A. M. van den Maagdenberg, D. Pietrobon, T. Pizzorusso, S. Kaja, L. A. Broos, T. Cesetti, R. C. van de Ven, A. Tottene, J. van der Kaa, J. J. Plomp, R. R. Frants and M. D. Ferrari, *Neuron*, 2004, 41, 701-710.
24. K. Eikermann-Haerter, E. Dilekoz, C. Kudo, S. I. Savitz, C. Waeber, M. J. Baum, M. D. Ferrari, A. M. van den Maagdenberg, M. A. Moskowitz and C. Ayata, *J Clin Invest*, 2009, 119, 99-109.
25. A. Tottene, R. Conti, A. Fabbro, D. Vecchia, M. Shapovalova, M. Santello, A. M. van den Maagdenberg, M. D. Ferrari and D. Pietrobon, *Neuron*, 2009, 61, 762-773.
26. A. A. Heemskerk, J. M. Busnel, B. Schoenmaker, R. J. Derks, O. Klychnikov, P. J. Hensbergen, A. M. Deelder and O. A. Mayboroda, *Anal Chem*, 2012, 84, 4552-4559.
27. E. Nevedomskaya, R. Derks, A. M. Deelder, O. A. Mayboroda and M. Palmblad, *Anal Bioanal Chem*, 2009, 395, 2527-2533.
28. C. A. Smith, E. J. Want, G. O'Maille, R. Abagyan and G. Siuzdak, *Anal Chem*, 2006, 78, 779-787.
29. R. Tautenhahn, C. Bottcher and S. Neumann, *BMC Bioinformatics*, 2008, 9, 504.
30. F. Dieterle, A. Ross, G. Schlotterbeck and H. Senn, *Anal Chem*, 2006, 78, 4281-4290.
31. C. A. Smith, G. O'Maille, E. J. Want, C. Qin, S. A. Trauger, T. R. Brandon, D. E. Custodio, R. Abagyan and G. Siuzdak, *Ther Drug Monit*, 2005, 27, 747-751.
32. D. S. Wishart, C. Knox, A. C. Guo, R. Eisner, N. Young, B. Gautam, D. D. Hau, N. Psychogios, E. Dong, S. Bouatra, R. Mandal, I. Sinelnikov, J. Xia, L. Jia, J. A. Cruz, E. Lim, C. A. Sobsey, S. Shrivastava, P. Huang, P. Liu, L. Fang, J. Peng, R. Fradette, D. Cheng, D. Tzur, M. Clements, A. Lewis, A. De Souza, A. Zuniga, M. Dawe, Y. Xiong, D. Clive, R. Greiner, A. Nazyrova, R. Shaykhutdinov, L. Li, H. J. Vogel and I. Forsythe, *Nucleic Acids Res*, 2009, 37, D603-610.

33. S. Naz, M. Vallejo, A. Garcia and C. Barbas, *J Chromatogr A*, 2014, 1353, 99-105.
34. W. B. Dunn, I. D. Wilson, A. W. Nicholls and D. Broadhurst, *Bioanalysis*, 2012, 4, 2249-2264.
35. T. Kind and O. Fiehn, *BMC Bioinformatics*, 2007, 8, 105.
36. L. W. Sumner, A. Amberg, D. Barrett, M. H. Beale, R. Beger, C. A. Daykin, T. W. Fan, O. Fiehn, R. Goodacre, J. L. Griffin, T. Hankemeier, N. Hardy, J. Harnly, R. Higashi, J. Kopka, A. N. Lane, J. C. Lindon, P. Marriott, A. W. Nicholls, M. D. Reily, J. J. Thaden and M. R. Viant, *Metabolomics*, 2007, 3, 211-221.
37. P. Hemstrom and K. Irgum, *J Sep Sci*, 2006, 29, 1784-1821.
38. B. Buszewski and S. Noga, *Anal Bioanal Chem*, 2012, 402, 231-247.
39. I. Kohler and D. Guillarme, *Bioanalysis*, 2014, 6, 1255-1273.
40. P. D. Rainville, G. Theodoridis, R. S. Plumb and I. D. Wilson, *TrAC*, 2014, 61, 181-191.
41. O. K. Argirov, N. D. Leigh and B. J. Ortwerth, *Ann N Y Acad Sci*, 2005, 1043, 903.
42. W. B. Dunn, A. Erban, R. J. M. Weber, D. J. Creek, M. Brown, R. Breitling, T. Hankemeier, R. Goodacre, S. Neumann, J. Kopka and M. R. Viant, *Metabolomics*, 2013, 9, S44-S66.
43. H. G. Gika, G. A. Theodoridis, R. S. Plumb and I. D. Wilson, *J Pharm Biomed Anal*, 2014, 87, 12-25.
44. G. R. Dalazen, M. Terra, C. E. Jacques, J. G. Coelho, R. Freitas, P. N. Mazzola and C. S. Dutra-Filho, *Metab Brain Dis*, 2014, 29, 175-183.
45. K. Sadilkova, S. M. Gospe, Jr. and S. H. Hahn, *J Neurosci Methods*, 2009, 184, 136-141.
46. A. Peduto, M. R. Baumgartner, N. M. Verhoeven, D. Rabier, M. Spada, M. C. Nassogne, B. T. Poll-The, G. Bonetti, C. Jakobs and J. M. Saudubray, *Mol Genet Metab*, 2004, 82, 224-230.
47. B. T. Poll-The and J. Gartner, *Biochim Biophys Acta*, 2012, 1822, 1421-1429.
48. S. Stockler, B. Plecko, S. M. Gospe, Jr., M. Coulter-Mackie, M. Connolly, C. van Karnebeek, S. Mercimek-Mahmutoglu, H. Hartmann, G. Scharer, E. Struijs, I. Tein, C. Jakobs, P. Clayton and J. L. Van Hove, *Mol Genet Metab*, 2011, 104, 48-60.
49. P. Baxter, *Biochim Biophys Acta*, 2003, 1647, 36-41.
50. B. Plecko, C. Hikel, G. C. Korenke, B. Schmitt, M. Baumgartner, F. Baumeister, C. Jakobs, E. Struys, W. Erwa and S. Stockler-Ipsiroglu, *Neuropediatrics*, 2005, 36, 200-205.
51. B. Plecko, S. Stockler-Ipsiroglu, E. Paschke, W. Erwa, E. A. Struys and C. Jakobs, *Ann Neurol*, 2000, 48, 121-125.
52. R. Bernasconi, R. S. Jones, H. Bittiger, H. R. Olpe, J. Heid, P. Martin, M. Klein, P. Loo, A. Braunwalder and M. Schmutz, *J Neural Transm*, 1986, 67, 175-189.
53. A. K. Charles, *Neurochem Res*, 1986, 11, 521-525.
54. M. C. Gutierrez and B. A. Delgado-Coello, *Neurochem Res*, 1989, 14, 405-408.
55. S. Matsumoto, S. Yamamoto, K. Sai, K. Maruo, M. Adachi, M. Saitoh and T. Nishizaki, *Brain Res*, 2003, 980, 179-184.
56. A. J. Beitz and A. A. Larson, *Eur J Pharmacol*, 1985, 114, 181-187.
57. Y. Kase, K. Takahama, T. Hashimoto, J. Kaisaku, Y. Okano and T. Miyata, *Brain Res*, 1980, 193, 608-613.
58. O. I. Klychnikov, K. W. Li, I. A. Sidorov, M. Loos, S. Spijker, L. A. Broos, R. R. Frants, M. D. Ferrari, O. A. Mayboroda, A. M. Deelder, A. B. Smit and A. M. van den Maagdenberg, *Proteomics*, 2010, 10, 2531-2535.

7. Figures captions

Fig. 1 Base peak electropherogram obtained by CE-ESI-MS for the analysis of 25 nL of precipitated mouse plasma. See Section 2.5 for experimental conditions.

Fig. 2 PCA score plots with experimental condition as a class identifier. A. Sham-operated group, B. CSD-operated group. Samples are colored according to their phenotype; RQ (red diamonds), plasma from transgenic mice carrying the FHM1 R192Q mutation; WT (blue diamonds), plasma from wild-type non-transgenic mice. t-scores represent the score vectors for the first (t[1]) and the second (t[2]) principal components after PCA. The first two principal components cover 48% and 42% of the total variability in A. and B., respectively.

Fig. 3 Cross-validated PLS-DA model and S-plot obtained from OPLS-DA regression. A. Cross-validated PLS-DA model built on CSD sub-group with R^2X cum = 0.417, R^2Y cum = 0.996, and Q^2 = 0.72; samples are colored according to their phenotype; RQ (red diamonds), plasma from transgenic mice carrying the FHM1 R192Q mutation; WT (blue diamonds), plasma from wild-type non-transgenic mice. B. S-plot obtained from OPLS-DA model. t-scores represent the cross-validated score vectors for the first (tcv[1]) and second (tcv[2]) principal components after cross-validated PLS-DA model.

Fig. 4 Box-plots displaying the differences in integrated peak areas observed for the two metabolites of interest after CSD events between the transgenic mice carrying the FHM1 R192Q mutation (labelled RQ) and the WT control group (labelled WT). Whiskers represent the standard deviation. A. *m/z* 130.0860, corresponding to pipecolic acid. B. *m/z* 147.1128, corresponding to lysine.

Fig. 5 Extracted ion chromatograms (EICs) and MS/MS spectra obtained for both compounds for standard solutions at 100 µg/mL (upper EIC) and prepared plasma sample (lower EIC). A. Pipecolic acid, product ion (PR) MS/MS experiments on *m/z* 130. B. Lysine, PR experiments on *m/z* 147. See Section 2.6 for experimental conditions.

Figure 1

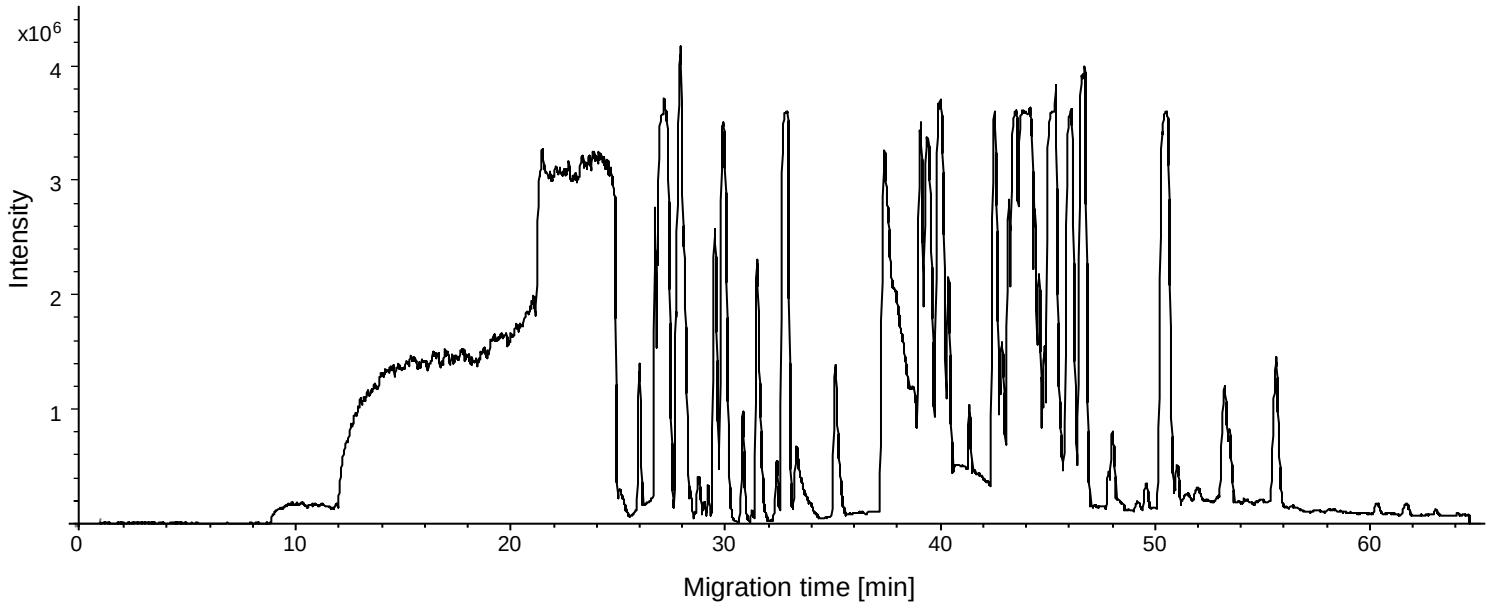

Figure 2

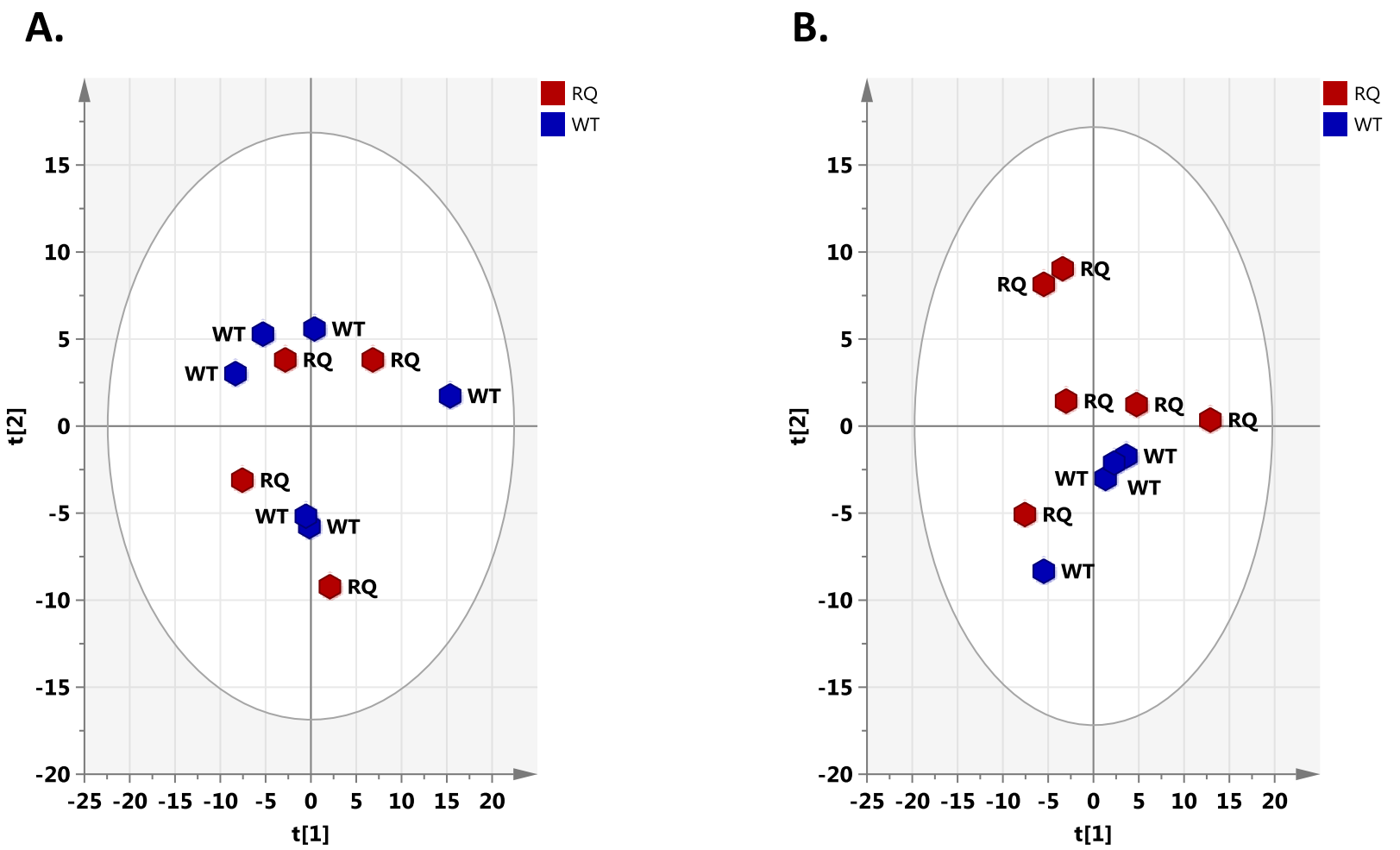

Figure 3

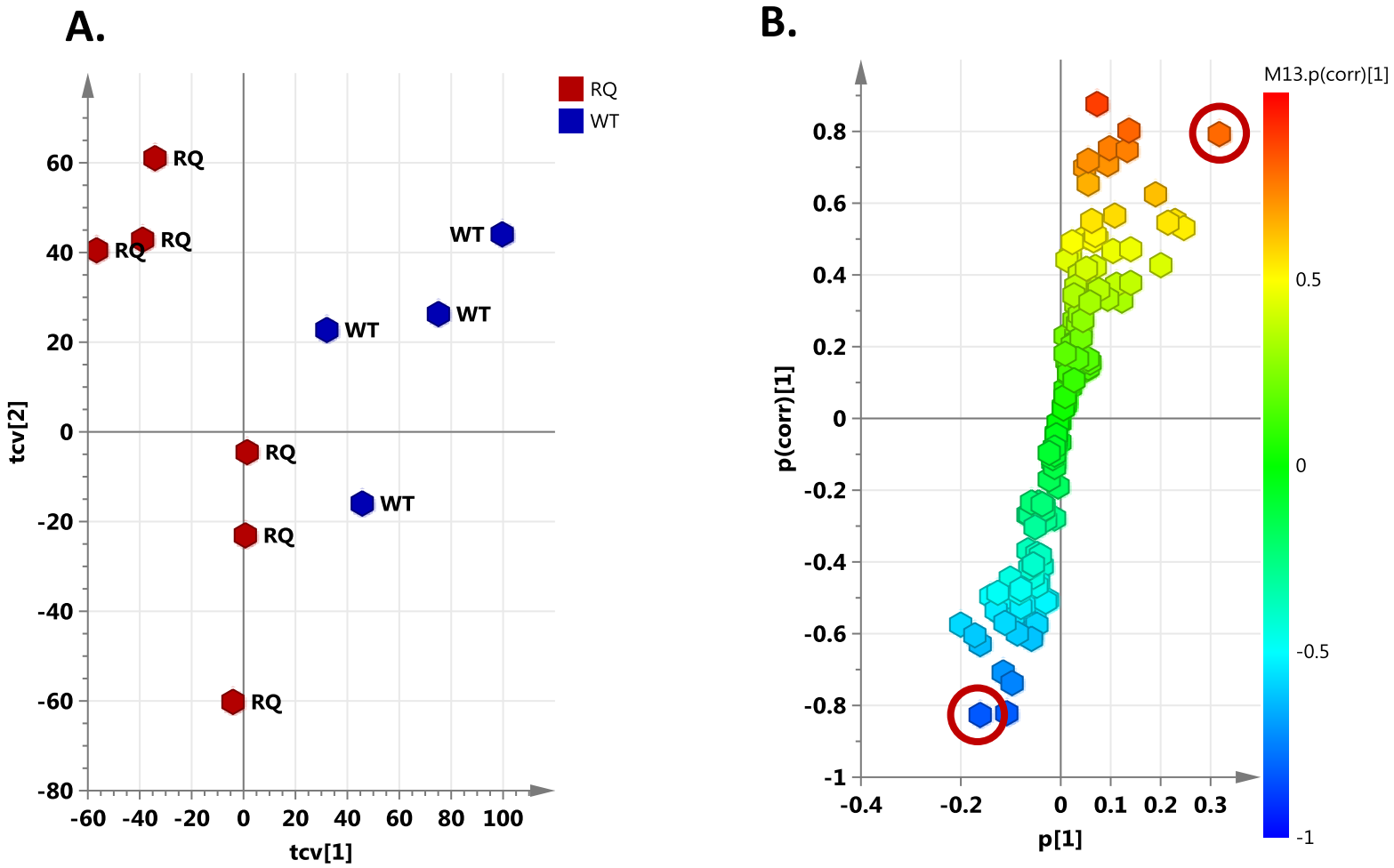

Figure 4

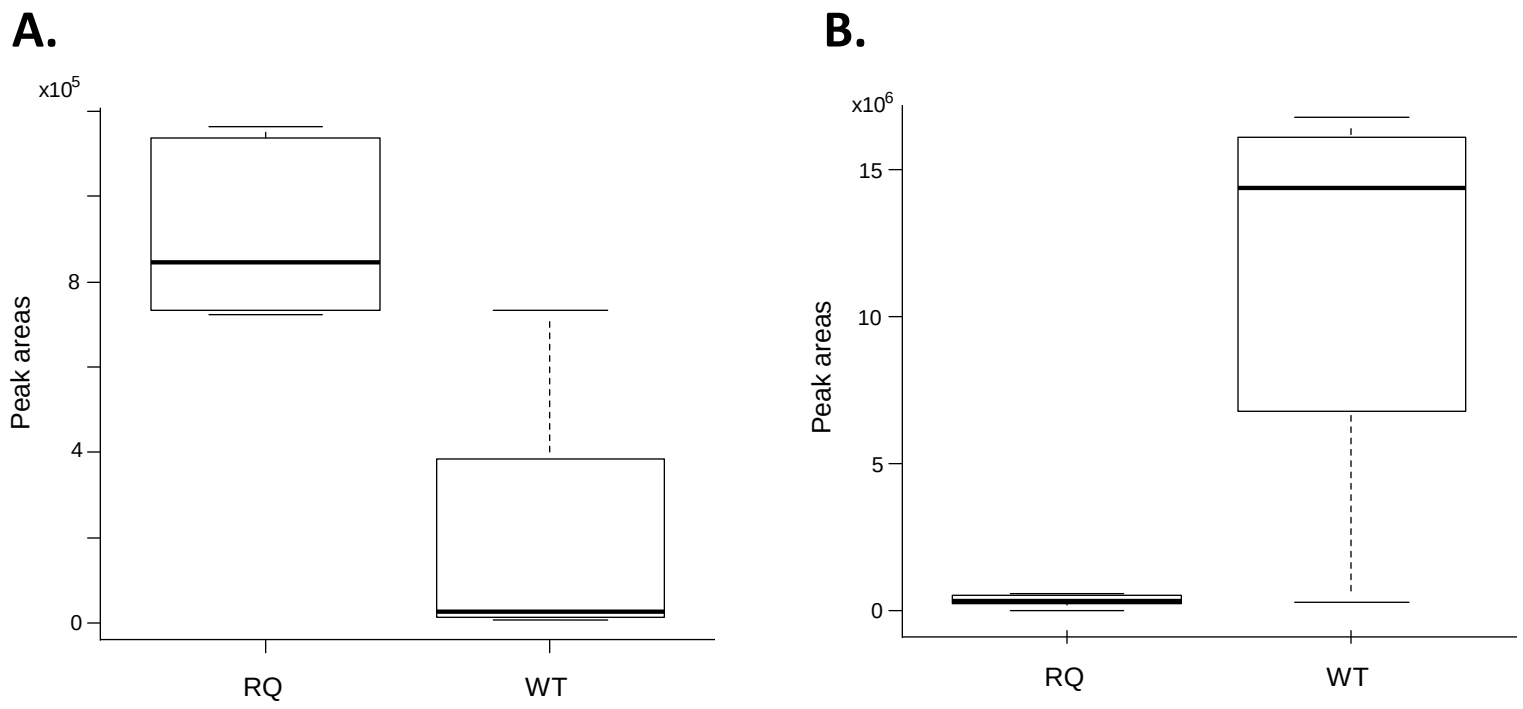

Figure 5